Heterogeneous & Homogeneous & Bio- & Nano-

CHEMCATCHEM

CATALYSIS

Accepted Article

Title: Understanding and Optimizing the Performance of Cu-FER for the Direct CH4 to CH3OH Conversion

Authors: Dimitrios Pappas, Elisa Borfecchia, Michael Dyballa, Kirill A. Lomachenko, Andrea Martini, Gloria Berlier, Bjørnar Arstad, Carlo Lamberti, Silvia Bordiga, Unni Olsbye, Stian Svelle, and Pablo Beato

To be cited as: *ChemCatChem* 10.1002/cctc.201801542

Link to VoR: http://dx.doi.org/10.1002/cctc.201801542

A Journal of

ChemPubSoc Europe

WILEY-VCH

www.chemcatchem.org

10.1002/cctc.201801542

WILEY-VCH

FULL PAPER

Understanding and Optimizing the Performance of Cu-FER for the Direct CH_4 to CH_3OH Conversion

Dimitrios K. Pappas,*[a] Elisa Borfecchia,[b, c] Michael Dyballa,[a, d] Kirill A. Lomachenko,[e] Andrea Martini,[c, f] Gloria Berlier,[c] Bjørnar Arstad,[d] Carlo Lamberti,[f, g] Silvia Bordiga,*[a, c] Unni Olsbye,[a] Stian Svelle,[a] and Pablo Beato*[b]

Abstract: Cu-exchanged zeolites with the Ferrierite topology were investigated in the direct CH_4 to CH_3OH conversion. Samples with a systematic compositional variation in terms of Na/Al and Cu/Al ratios where synthesized by liquid ion exchange. The presence of Na is observed to be beneficial for the Cu exchange and thereby higher Cu loadings were achieved. The overall performance of Cu-FER samples depends on Cu loading as well as the conditions of the reaction. Elevated O_2 activation temperature as well as long CH_4 loading times are proven to enhance the CH_3OH yield of the Cu-FER sample with Cu/Al = 0.2. In addition, the productivity depends on the Cu/Al ratio, at low values the sample is almost inactive indicating a Cu threshold that needs to be surpassed. We employed X-ray absorption and IR of adsorbed CO spectroscopies in order to rationalize the performance as well as the effect of Cu/Al ratio. From the *in situ* spectroscopies we ultimately establish structure-activity relationships between the reducibility of Cu species and the CH_3OH yield.

[a] Dimitrios K. Pappas, Dr. Michael Dyballa, Prof. Silvia Bordiga, Prof. Unni Olsbye, Prof. Stian Svelle
Center for Materials Science and Nanotechnology (SMN), Department of Chemistry
University of Oslo
1033 Blindern, 0315 Oslo, Norway
E-mail: dimitrios.pappas@smn.uio.no
[b] Dr. Elisa Borfecchia, Dr. Pablo Beato
Haldor Topsøe A/S
Haldor Topsøes Allé 1, 2800 Kongens Lyngby, Denmark
E-mail: pabb@topsoe.com
[c] Dr. Elisa Borfecchia, Andrea Martini, Dr. Gloria Berlier, Prof. Silvia Bordiga
Department of Chemistry, NIS Centre and INSTM Reference Center
University of Turin
via P. Giuria 7, 10125 Turin, Italy
E-mail: silvia.bordiga@unito.it
[d] Dr. Michael Dyballa, Dr. Bjørnar Arstad
SINTEF Industry
Forskningsveien 1, 0373 Oslo, Norway
[e] Dr. Kirill Lomachenko
European Synchrotron Radiation Facility (ESRF)
71 avenue des Martyrs, CS 40220, 38043 Grenoble Cedex 9, France
[f] Andrea Martini, Prof. Carlo Lamberti
Smart Materials, Research Institute
Southern Federal University
Sladkova Street 174/28, 344090 Rostov-on-Don, Russia
[e] Prof. Carlo Lamberti
Department of Physics, CrisDi Interdepartmental Center
University of Turin,
via P. Giuria 1, 10125 Turin, Italy

Supporting information for this article is given via a link at the end of the document.

Introduction

The direct conversion of CH_4 to CH_3OH bypassing the syngas route can potentially provide a feasible and sustainable pathway for the utilization of this abundant energy source.[1] Cu-exchanged zeolites have the ability to cleave the C-H bond of CH_4 and, via hydrolysis, transform it to CH_3OH.[1a, 2] The conversion is a stepwise stoichiometric process, which currently is far from commercial realization. Initially the materials are activated at high temperature, typically above 400 °C, in the presence of O_2 leading to the formation of Cu-oxo species.[3] Then CH_4 is loaded at lower temperature (200 °C) and finally CH_3OH is extracted online by introducing steam to the reactor.[2b, 2c, 3a, 4]

Different zeolites are known to possess the active Cu site motifs capable of the conversion. Cu-MOR,[2a-c, 2f, 4-5] Cu-ZSM-5[5a, 5g, 6] and Cu-SSZ-13[3a, 4, 5g, 7] exhibit high yields with the maximum being 0.47,[2f] 0.21[6a] and 0.172[3a] ($molCH_3OH/molCu$) for each topology respectively. Due to the stoichiometric nature of the process, the CH_3OH output is inevitably dictated by the density and nuclearity of the active sites.

Cu-FER zeolites have been investigated in the past as active catalysts for SCR of NO_x.[8] However, only a few reports on their activity in the CH_4 to CH_3OH conversion exist.[2d, 5c, 9] The reported CH_3OH productivities for Cu-FER are substantially smaller than those seen for the most productive zeolites. Clearly, there is potential to increase the activity of the materials through a fundamental understanding of the active sites and a consequent optimization of material preparation procedures as well as reaction conditions.

The FER structure possesses multiple cationic sites (Figure 1).[8a, 10] Cu^I ions have been located in the walls of the main (M) 10-member ring (10r) and perpendicular (P) 8-member ring (8r) channels as well as at their intersection (I).[10-11] The binding energy of Cu^I ions on the wall of both channels was found to be lower compared to the intersection.[10b] The location of Cu^{II} ions was studied experimentally by XRD and ESR spectroscopy[8a] and using DFT calculations.[11] Initially, the intersection (I) of 8r and 10r channels was proposed as a site for weakly coordinated Cu^{II} ions highly accessible to reactants.[8a] Later, Sklenak et al. located Cu^{II} ions in the 6-member ring (6r), in the wall of the main 10r channel (M) formed by two 5-member rings (5r), and in the deformed 6r in the perpendicular 8r channel of FER (P).[11] The 8r channel site was reported to be preferentially populated due to a

higher Cu^{II} binding energy, depending on the Al siting, compared to the one in the main channel, making the latter more reactive.[11]

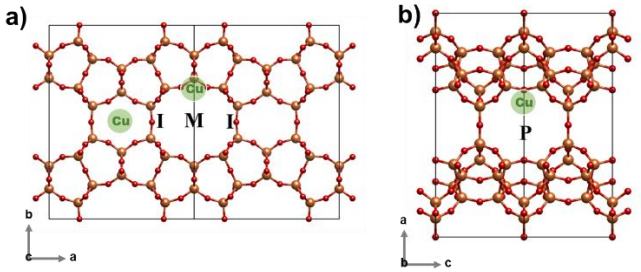

Figure 1. Cu^{II} locations in the FER framework as discussed in literature.[8a, 11] Three distinct locations have been identified, namely: the intersection (I) of 8r-member ring (8r) and 10r-member ring (10r) channels, the 6-member ring (6r) in the wall of the main 10r channel (M) and in the deformed 6r in the perpendicular 8r channel of FER (P). a) view of the framework along c-axis and b) along b-axis.

Herein we investigate Cu-FER samples prepared from the H- and Na-containing parent material with different Cu/Al ratios. In addition, we study different reaction conditions for the direct CH_4 to CH_3OH conversion, namely O_2 activation temperature and CH_4 loading time in order to maximize CH_3OH the yield of the Cu-FER prepared using different procedures. The materials were studied by the means of *in situ* High Energy Resolution Fluorescence Detected X-Ray Absorption Near Edge Structure (HERFD XANES) spectroscopy[12] as well as Infrared (IR) spectroscopy[13] attempting to rationalize their behavior and establish structure-activity relationships.

Results and Discussion

Physicochemical Characterization

The materials were prepared from the H- or Na-forms of the parent FER zeolite. Cu was introduced via Liquid Ion Exchange (LIE) (see Experimental section for details). The H-FER could not be exchanged with high copper amounts (above Cu/Al = 0.11) due to strong diffusion limitation and CuO aggregate formation limiting the copper content achievable. The H,Na-FER(11), obtained by partially exchanging the H-FER(11) with sodium ions, allowed us to achieve higher loadings. The obtained Cu/Al ratio ranges from 0.11 to 0.20; also in this case, higher Cu loadings led to the formation of Cu nanoparticles instead of ion exchange. Table 1 summarizes the sample nomenclature, synthesis method, compositional characteristics, N_2-physisorption results and H_2O content of the investigated zeolites.

After synthesis, the samples were subjected to basic physicochemical characterization, i.e. SEM, EDS, TGA, XRD, BET and ^{27}Al MAS NMR, as detailed in the experimental section and Supporting Information (SI). A very small amount of extra-framework Al was identified in all materials by ^{27}Al MAS-NMR. We note that extra-framework Al is not increasing upon cation exchange; rather a small realumination can be observed. Interestingly the amount of Na in the H,Na-FER(11) decreased upon Cu exchange indicating the preferential exchange of Cu with Na cations (rather than protons). Very few nanoparticles with an average size of 50 nm were seen using SEM for the high loading sample (i.e. 0.20Cu-H,Na-FER-(11)). The contribution of these minor aggregates over the total Cu can be neglected. Indeed, even using high-energy resolution XANES, no traces of metal Cu or bulk-like $Cu^{II}O$ were observed.

Direct CH_4 to CH_3OH Conversion

The synthesized Cu-FER samples were investigated for the direct CH_4 to CH_3OH conversion. Reaction protocols and experimental procedures are described in the Experimental section and summarized in Table 2. Based on our previous work,[3a] we initially investigated the effect of reaction conditions over 0.20Cu-H,Na-FER(11); the results are depicted in Figure 2.

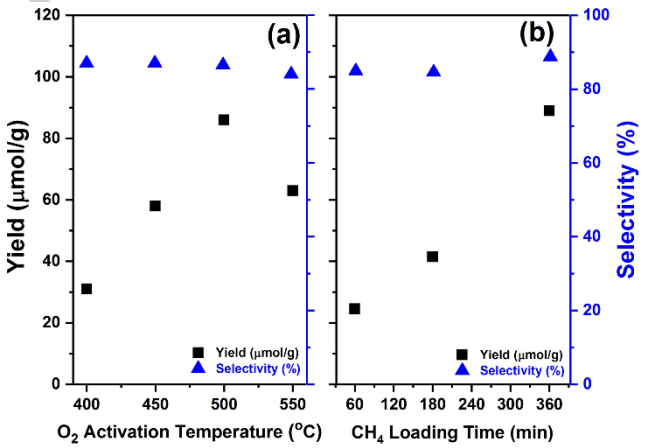

Figure 2. (a) Effect of O_2 activation temperature on the CH_3OH yield (µmol/g_{cat}) (left axis, black squares) and selectivity (%) (right axis, blue triangles) for 0.20Cu-H,Na-FER(11) sample. The reaction conditions are identical to Table 2 except for the activation temperature which was varied from 400 to 550 °C. (b) Effect of CH_4 loading time (min) on the CH_3OH yield (µmol/g_{cat}) (right axis, black squares) and selectivity (%) (left axis, blue triangles) for 0.20Cu-H,Na-FER(11) sample. The reaction conditions are also identical to Table 2 except the CH_4 loading time.

Table 1. Properties of parent and Cu-exchanged samples determined by EDX, N_2-physisorption and TGA

Sample	Exchange Method	Si/Al[1]	Cu/Al[1]	Na/Al[1]	Cu [wt%][1]	BET [m^2/g]	V_{tot} [ml/g][2]	V_m [ml/g]	H_2O (wt. %)
H-FER	-	11	-	-	-	431	99	0.244	
0.10Cu-H-FER(11)	LIE, 0.02 M	11	0.11	-	1.00	483	111	0.263	7.7
H,NaFER	-	11	-	0.40	-	422	97	0.236	
0.14Cu-H,Na-FER(11)	LIE, 0.005 M	11	0.14	0.17	1.46	444	102	0.255	7.5
0.20Cu-H,Na-FER(11)	LIE, 0.02 M	11	0.20	0.16	1.86	356	82	0.218	7.4

[1] determined by EDX [2] determined at $p/p_0 = 0.99$

Higher O_2 activation temperature has been shown to increase the yield for Cu-CHA[3a] and Cu-MOR.[3b, 5c] Analogous observations were made here: an increment in productivity of 56 µmol/g is observed when moving from 400 to 500 °C (Figure 2a). Interestingly further increase of the temperature to 550 °C resulted in a decrease in the yield; similar results have been observed for other Cu-exchanged frameworks attributed to Cu clustering aided at very high temperatures.[5c] This volcano type behavior indicates that for Cu-FER samples 500 °C is the optimum O_2 activation temperature. Likewise, increased time of CH_4 loading leads to a yield enhancement (Figure 2b). High activation temperature and prolonged reaction time, can explain the higher yields seen here compared to the literature, where low O_2 activation temperatures (450 °C),[9] short reaction times with CH_4 (30 min),[5c] and low CH_4 partial pressure[9] (i.e. 50 mbar) were used.

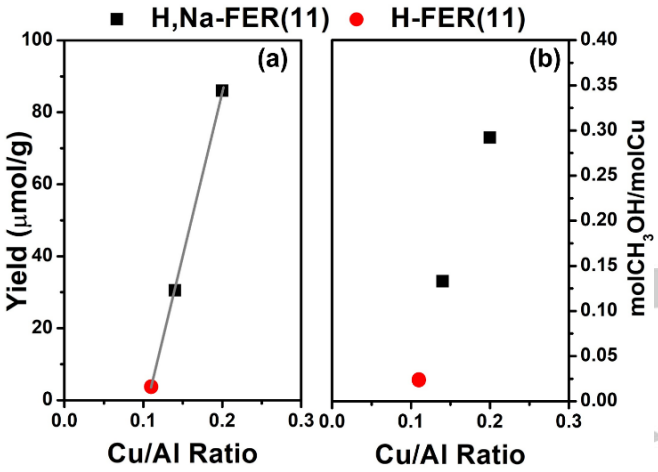

Figure 3. CH_3OH output over Cu-FER with different Cu/Al ratio under identical reaction conditions (see Table 2) (a) CH_3OH yield in µmol/g (b) normalized yield with respect to Cu content in molCH_3OH/molCu. Red circle represents the material derived from H-FER(11) while black squares correspond to H,Na-FER(11) derived samples. The selectivity of the samples is illustrated in Figure S4 in the SI.

At increasing Cu loading of Cu-FER, a linear increase in the yield is observed (Figure 3a). The sample with the lowest Cu/Al ratio, 0.11Cu-H-FER(11), exhibits a very low CH_3OH yield of 3.8 µmol/g. On the other hand, 0.20Cu-H,Na-FER(11) gives the highest CH_3OH yield (88 µmol/g). The selectivity remained above 80% for all the tested samples (Figure S4 in the SI). From a linear fit of the data in Figure 3a, an intersection with the x-axis at Cu/Al = 0.1 is extracted. This indicates that the first exchanged Cu ions occupies inactive positions in the framework. The need to saturate inactive sites before active ones can be populated is a behavior already observed in some catalysts.[14] Normalizing the yield with respect to the Cu loading (Figure 3b) it is demonstrated that increasing the Cu loading indeed leads to an increase of the amount of active Cu. In the case of Cu-MOR[2b, 4] and Cu-ZSM-5[6a] the molCH_3OH/molCu has been reported not to depend on the Cu loading. However, Cu-CHA exhibited a similar effect at low Cu/Al ratio as seen for Cu-FER, which was explained by the coordination of Cu ions in the very stable 2Al 6r positions as bare Cu^{II}, making the Cu species inactive for the conversion.[3a, 15]

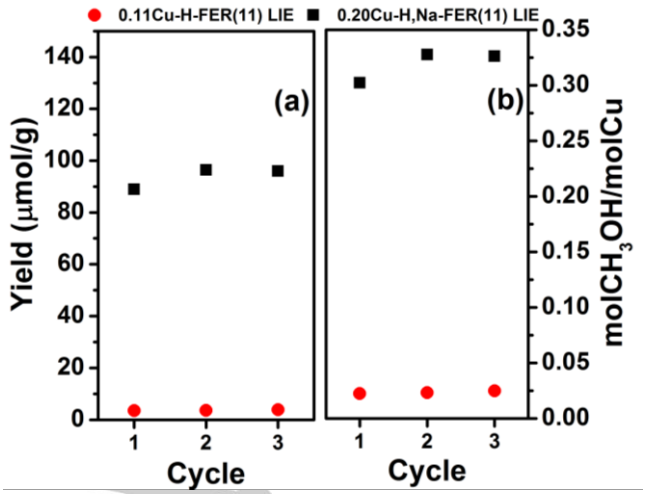

Figure 4. Multiple reaction cycles over 0.11Cu-H-FER(11) and 0.20Cu-H,Na-FER(11) samples, each reaction cycle was performed according to the conditions in Table 2. Between each cycle the sample was purged with He for 3h at 200 °C. (a) CH_3OH yield in µmol/g_{cat}; (b) normalized yield with respect to Cu content in molCH_3OH/molCu.

The 0.11Cu-H-FER(11) and 0.20Cu-H,Na-FER(11) samples were subjected to multiple reaction cycles, to investigate their reusability (Figure 4). The results indicate that the materials do not deteriorate with cycling. The performance of the low loading sample i.e. 0.11Cu-H-FER(11) is not affected by the cycles, within the experiment sensitivity. Conversely the high loading 0.20Cu-H,Na-FER(11) exhibits a small yield increment finally reaching a value of 0.33 molCH_3OH/molCu making it comparable to highly active Cu-MOR. [2b, 16] The yield increment has been reported to be linked to the mobility of Cu ions during hydration and the final stabilization after high temperature activation in more active positions.[3a, 17]

In situ HERFD XANES Measurements

In situ HERFD XANES was employed to assess the oxidation state and average coordination of Cu-FER under characteristic pre-treatments. The spectra were collected at the ID26 beamline of the European Synchrotron Radiation Facility (see Experimental section for details). Three distinct pre-treatments were employed over 0.20Cu-H,Na-FER(11), namely He activation (He Act.) at 500 °C, reaction with O_2 at 500 °C of the He-activated sample (He Act. + O_2) and O_2 activation (O_2 Act) also at 500 °C. The spectra are reported after stabilization of the XAS features while productivity of the materials (Figure 5 bottom inset) was measured after activation for 8 h in a fixed bed laboratory reactor (see Experimental section). The different activation times for laboratory tests (longer activation to enhance the productivity) and HERFD XANES experiments (shorter activation, dictated by the limited beam time availability) allow relevant qualitative correlations but hinder quantitative ones. Figure 5 depicts the

characteristic XANES features of the investigated Cu-zeolites which were interpreted on the basis of the current Cu K-edge XANES literature.[3a, 5g, 5h, 15, 18]

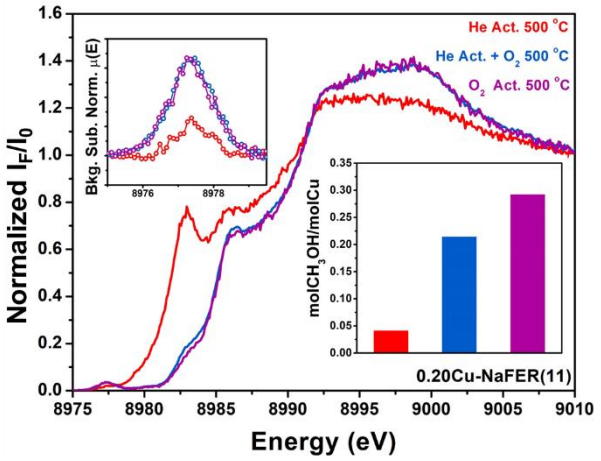

Figure 5. Cu K-edge HERFD XANES of 0.20Cu-H,Na-FER(11) after different activations, namely He activation at 500 °C (red line), reaction with O_2 at 500 °C of the He-activated sample (blue line) and O_2 activation at 500 °C (purple line). The background subtracted 1s→3d pre-edge peak characteristic of Cu^{II} ions is shown in the top inset. The bottom right inset depicts the molCH₃OH/molCu.

He Act. results in a Cu^{I}-containing state as indicated by the pronounced peak at 8983 eV corresponding to the 1s→4p transitions of Cu^{I} ions at lower energy compared to Cu^{II}. The final state of He Act., is a result of framework dehydration as well as the so called ''self-reduction'' of Cu species.[3a, 18a, 19] This evolution was followed by time-resolved measurements illustrating the development of the peak at 8983 eV as well as the decreasing intensity of the White Line (WL) (see Figure S6). It is noteworthy that some Cu^{II} species withstand the ''self–reduction''; these are evident by the peak 8986 eV assigned to 1s→4p transitions of Cu^{II} ions as well the pre-edge peak at 8977 eV of dipole-forbidden but quadrupole allowed 1s→3d transitions of Cu^{II} ions (Figure 5 top inset). Similar observations have been made for tightly coordinated Cu species in 6r of CHA[3a] and SZR[20] where Cu sits as inactive $2AlZ_2Cu^{II}$ in 6r. He Act. at high temperature is observed to result in low yields of CH_3OH [3a, 7b] (Figure 5 bottom inset). The residual activity is possibly connected to O-ligated multicopper species surviving the reduction.[3a, 7b]

O_2 Act. on the other hand, results in a dominant Cu^{II} state evident from the marked rising edge shoulder at 8986 eV and the well-defined pre-edge peak (Figure 5 top inset). Furthermore, the average coordination number of Cu is higher in this case compared to the He Act. case, as supported by the increased WL intensity. This state of the material is linked to high CH_3OH yield (Figure 5 bottom inset). O_2 is essential for the formation and/or stabilization of active Cu_xO_y moieties. He Act. + O_2 at 500 °C was finally employed to decouple dehydration/''self-reduction'' from the reaction with O_2. The corresponding yield as well as the XANES spectrum are depicted in Figure 5. The spectrum is almost identical to the one collected after O_2 activation. Small differences, indicated by grey arrows in Figure 5, suggest the presence of a minor fraction of residual Cu^{I} species (peak at 8983 eV), reflected also to a lower yield (Figure 5 bottom inset).

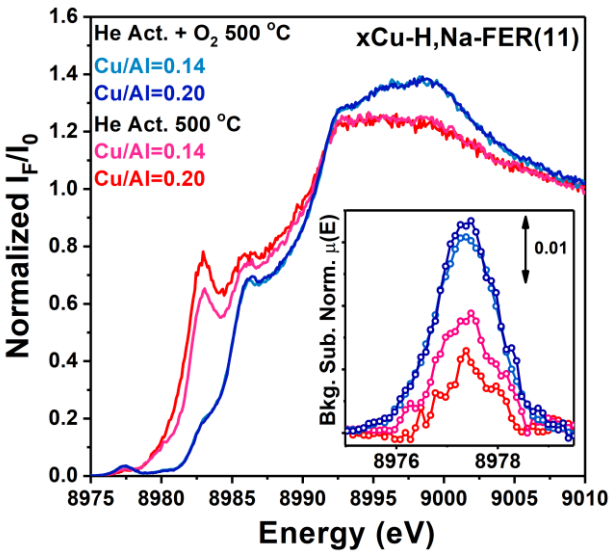

Figure 6. Cu K-edge HERFD XANES of 0.14Cu-H,Na-FER(11) and 0.20Cu-H,Na-FER(11) after He activation at 500 °C and He activation at 500 °C followed by reaction with O_2 at the same temperature. The inset reports the background subtracted normalized intensity of the 1s→3d pre-edge peak characteristic of Cu^{II} ions

In situ HERFD-XANES was also utilized to study the effect of Cu/Al ratio in the oxidation state and average Cu coordination (Figure 6). Focusing on the spectra obtained after He Act. + O_2 at 500 °C, both materials exhibit very similar XANES spectra. In detail, the Cu^{II} peak at 8986 eV and the 1s→3d pre-edge peak (Figure 6 inset) appear faintly suppressed in the case of 0.14Cu-H,Na-FER(11), although this evidence alone cannot explain the different performance. Recently, we linked the reducibility of Cu-CHA zeolites to the CH_3OH productivity.[3a] In a similar manner, here we compare the He-activated state of the Cu-H,Na-FER with Cu/Al of 0.20 and 0.14. Under these pre-treatment conditions, we are able to access the degree of ''self-reduction''. The difference in the intensity of the 1s→4p peak corresponding to Cu^{I} ions at 8983 eV is apparent. The intensity of the rising edge peaks can be affected by the coordination geometry of the Cu species.[21] Nonetheless, the very similar shape of the overall XANES spectrum for the two materials suggests that the same Cu^{I} coordination motif is maintained. The best descriptor for the oxidation state of the materials, less perturbed by the shape of the rising edge, is the pre-edge 1s→3d peak (Figure 6 inset), which also points towards the same observation, i.e. a higher degree of self-reduction at higher Cu-loading.

It appears that Cu locations in FER possess different redox barriers modifying their reducibility and activity. Here the more reducible sample (0.20Cu-H,Na-FER) exhibits the highest activity in the reaction. The reducibility stems from the different coordination environments associated to positions of Cu in the framework, reported to show different binding

energies.[11] This difference can potentially lead to preferential population of these sites, as also hinted by the limit of Cu/Al=0.1 which is to be surpassed in order to form active Cu motifs (Figure 3a).

In situ IR of Absorbed CO

To further quantify the amount of reducible Cu species we employed IR spectroscopy of adsorbed CO, that probes only Cu^{I}, and not Cu^{II}, species.[22] The spectra obtained at different CO pressures P_{CO} samples (low, medium and high) over vacuum activated samples are illustrated in Figure 7 and Figure S8, at RT and at liquid nitrogen temperature (LNT), respectively. For the latter, mono-, di- and tri-carbonyl adducts are identified.[13, 23] The interaction of Brønsted sites and of Na^{+}, with CO originating from protons and un-exchanged Na^{+} are also evident in Figure S8. The di- and tri-carbonyl species appear more developed in the case of the 0.20Cu-H,Na-FER(11).

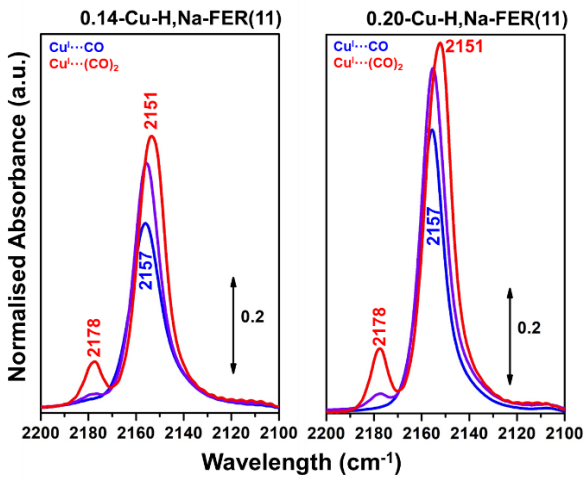

Figure 7. IR spectra of CO dosed at RT on 0.14Cu-H,Na-FER(11) and 0.20Cu-H,Na-FER(11). Blue, purple and red lines correspond to low, medium and high P_{CO}. The samples where activated in vaccuo at 150 °C for 1h, 300 °C for 1h and 450 °C for 1h.The spectra are background subtracted and are normalized with respect to the zeolite framework vibrational modes as well as to the Cu wt.%.

The RT spectra, usually less informative than the LNT ones, have been considered here to avoid the contribution of Brønsted sites and Na^{+} ions. At low P_{CO} a peak at 2157 cm^{-1} evident for both samples is assigned to monocarbonyl species (Cu^{I}···CO). Two more peaks at 2178 cm^{-1} and 2151 cm^{-1} are observed after increasing the CO pressure. The peasks are assinged to symmetric and asymmetric CO stretching modes of dicarbonyl species Cu^{I}···$(CO)_2$ respectively.It is clear that the sample with higher Cu loading can host, per Cu ion, more CO molecules both as mono- and di-carbonyl copper complexes. Qualitatively these results suggest that 0.20Cu-H,Na-FER(11) contains more under-coordinated, accessible Cu^{I} species having three or two oxygen framework neighbors.[23] This enables the formation of active Cu_xO_y motifs compared to tightly framework-coordinated Cu ions upon interaction with O_2.

Conclusions

In summary, Cu-FER zeolites were thoroughly investigated as attractive materials for the CH_4 to CH_3OH reaction. The Cu/Al ratio appears to influence their performance. Higher activation temperature and longer CH_4 loading time both positively influenced the yield. He act. results to no substantial CH_3OH amounts due to the absence of oxidized Cu species. On the other hand, reaction of O_2 with previously reduced sample at 500 °C resulted in a large fraction of active Cu, comparable to O_2 activation. *In situ* HERFD XANES as well as IR spectroscopy of adsorbed CO were employed on Cu-H,Na-FER samples and indicated that the Cu loading influences the reducibility and ultimately the reactivity. From these results and previous findings,[8a, 10b, 11, 23] we suggest that at low loading Cu ions prefer positions where they are tightly coordinated to framework oxygen and are more energetically stable, thus less reactive. Increasing the Cu loading, these sites are saturated and and sites with lower coordination number and higher redox potential and reactivity are occupied, possibly positioned in the wall of the main 10r channel. In order to fully identify the nature and location of the active sites for the CH_4 to CH_3OH conversion in Cu-FER advanced characterization coupled with DFT calculations will be required.

Experimental Section

Synthesis

The zeolite (NH_4-FER) was received from Zeolyst (CP914). Initially the material was calcined for 12 h at 550 °C (ramp 1 °C/min) to remove carbon residues. The material was then exchanged at 60 °C, three times with a solution of 10 wt. % NH_4NO_3 or 5 times with a solution of $NaNO_3$ and washed with demineralized water until nitrate-free. To get the H-form of the material ammonia was burned off by calcining the sample at 500 °C for 8 h (ramp 1 °C /min). These resulted in parent samples H-FER(11) and H,Na-FER(11) respectively.

For the Liquid Ion Exchange (LIE) with copper(II) acetate ($CuAc_2$, Sigma-Aldrich) the salt was diluted in distilled water (concentration 0.02 and 0.005 M for H,Na-FER(11) while 0.02 M for H-FER(11), see Table 1). The parent material was added to the solution (60 ml/g) and the pH was adjusted in the range of 5.2 – 5.7 using NH_4OH solution (28 wt.%, Sigma-Aldrich) in order to avoid copper precipitation. The samples were stirred at RT for 16 h, finally the solution was removed by centrifugation and the samples were washed at least three times to remove surplus copper ions.

Laboratory Physicochemical Characterization

Nitrogen physisorption at 77K was performed on a BELSORP-minII instrument. Initially the materials were treated in vacuum at 80 °C for 1 h and at 300 °C for 2 h. The specific surface area of the samples was calculated using the Brunauer-Emmett-Teller (BET) equation.[24] Scanning Electron Microscopy (SEM) images were collected on a Hitachi SU8230 instrument. The elemental composition, was determined by Energy-Disperse X-Ray (EDX) spectroscopy at 20 kV accelerating voltage on

200x200 µm areas of the sample. Bruker Quantax system consisting of a XFlash 6T|10 detector and Espirit was utilized for the quantification. Thermogravimetric Analysis (TGA) (Stanton Redcroft) was used in order measure the H_2O content of the zeolites. The material was heated with a 1 °C/min rate to 300 °C and that temperature was maintained for 90 min. The H_2O content of the Cu containing materials is tabulated in Table 1 and was used for the correction of sample mass during the quantification of the conversion products.

Direct CH_4 to CH_3OH Conversion

The performance of Cu-FER zeolites in the CH_4 to CH_3OH conversion was tested in a quartz plug flow reactor (I.D. = 6 mm). A uniform particle distribution in the range of 425 to 250 µm was obtained by pressing, crushing and sieving the powders, then 100 mg were packed in the reactor. A tubular oven was used to control the temperature during the reaction, monitored by a thermocouple. Initially the samples were dried in helium flow (15 ml/min) at 150 °C; then O_2 flow (15 ml/min) was introduced and the temperature was increased (ramp 5 °C/min) to 500 °C for 480 min. After activation, the temperature was decreased (ramp 5 °C/min) to 200 °C in O_2. The catalyst was then purged with He for 60 min. During CH_4 loading, 15 ml/min of CH_4 were introduced for 360 minutes at 200 °C. Finally, the sample was purged again with He before the isothermal online extraction of CH_3OH with 15 ml/min 10% H_2O steam and the effluent was analyzed by a Hewlett Packard 6890/5972 GCMS System where CH_3OH, CH_3OCH_3 and CO_2 were the main products detected (CH_3OCH_3 was accounted as two CH_3OH molecules). The experimental conditions are summarized in Table 2 below.

Table 2. Reference conditions for the direct CH_4 to CH_3OH conversion.

Process Step	Temperature (°C)	Gas Composition	Flow (ml/min)	Time (min)
O_2 Activation	500	100% O_2	15	480
CH_4 Loading	200	100% CH_4	15	360
H_2O Assisted Extraction	200	10% H_2O in Ne/He	15	70

For the characteristic activation experiments reported in Figure 5, namely He activation at 500 °C, He activation and subsequent reaction with O_2 at 500 °C and O_2 activation at 500 °C, the activity tests were performed as follows. The samples were initially treated in He (He act. at 500 °C and He act. + O_2 at 500 °C) or O_2 (O_2 act. at 500 °C) for 480 min. In the case of He act. + O_2 at 500 °C the O_2 flow was introduced after the aforementioned time in He at 500 °C for 30 min. The materials were then cooled down to 200 °C where CH_4 loading took place for 360 min. Afterwards the materials were flushed with He and extraction took place isothermally (i.e 200 °C) with 10 % H_2O containing steam. The long activation times were employed to enhance the CH_3OH yield, while in the case of the HERFD-XANES measurements the spectra were acquired until the relative stabilization of the features due to the limited available beamtime.

High-Energy Resolution Fluorescent Detection X-Ray Absorption Spectroscopy (HERFD XANES)

Cu K-edge High-Energy Resolution Fluorescent Detection X-Ray Absorption Spectroscopy Near Edge Structure (HERFD XANES)[12, 25] measurements were conducted at the ID26 beamline of the European Synchrotron Radiation Facility (ESRF, Grenoble, France). HERFD XANES spectra were collected in fluorescence mode detecting only photons with energy corresponded to the maximum intensity of the Cu $K\beta_{1,3}$ emission line at ca. 8906 eV. To this aim, five Si(553) analyzer crystals in vertical Rowland geometry were employed, focusing the X-ray fluorescence radiation on an Avalanche Photodiode (APD) detector. To select the energy of the incident X-ray beam, a flat double-crystal Si(311) monochromator was employed.

In situ HERFD XANES measurements following O_2 activation as well as He activation and subsequent reaction of the reduced sample with O_2 of 0.14Cu-H,Na-FER(11) and 0.20Cu-H,Na-FER(11), were performed using the Microtomo reactor cell[26] designed by the ESRF Sample Environment Group, attached to a gas-flow setup.[18a, 18f] The zeolites were pressed into self-supplementary wafers of ca. 100 mg and fixed inside the reaction cell. For the different pretreatments the samples were heated from room temperature (RT) to 500 °C (ramp 5 °C/min) under a 100 ml/min flow of the corresponding gas. Moisture traps were employed to prevent any unwanted water contamination. During temperature ramps 2 min scans were employed in order to follow the time and temperature evolution of the XANES features. After stabilization of the XANES features of the samples at the activation temperature, we collected 5 scans, which were averaged after checking for signal reproducibility to obtain for each sample a HERFD XANES spectrum representative of the final activated state. Regarding the experimental data reduction, HERFD XANES were treated in the same way as the conventional one, using the PyMCA software[27] for initial visualization and export of the scans and then the Athena software[28] for averaging and normalization to the edge-jump.

FTIR Measurements

FTIR measurements were performed in transmission mode on a Bruker Vertex 80 instrument with a Mercury-Cadmium-Telluride (MCT) detector. A quartz cell with KBr windows was employed. The fresh catalyst was prepared as thin wafers, self-supported in a gold envelope and pre-treated under vacuum at 150 °C for 1h, 300 °C for 1h and 450 °C for 1h. CO adsorption measurements were conducted at room as well as liquid nitrogen temperature. CO was dosed in the sample in order to follow the evolution of different CO adducts with increasing pressure. The collected spectra of the H,FER(11), H,Na-FER(11) and Cu loaded samples namely 0.14Cu-H,Na-FER(11) and 0.20Cu-H,Na-FER(11) were normalized with respect to the framework vibration modes intensity. The obtained spectra at 25 °C as well as -196 °C (LNT) are depicted in Figure 7 in the main text and Figure S8 respectively.

Acknowledgements

This publication forms a part of the iCSI (industrial Catalysis Science and Innovation) Centre for Research-based Innovation, which receives financial support from the Research Council of Norway under contract no. 237922. EB acknowledges Innovation Fund Denmark (Industrial postdoc n. 5190-00018B). CL and AM acknowledge the Mega-grant of the Russian Federation Government to support scientific research at the Southern Federal University, No. 14.Y26.31.0001. Dr. Rafal Baran is kindly acknowledged for his assistance during the experiment at ID26 beamline of the ESRF.

Keywords: Cu-exchanged ferrierite • direct methane to methanol conversion • HERFD XANES • IR • structure-activity relationships

[1] a) M. Ravi, M. Ranocchiari, J. A. van Bokhoven, *Angew. Chem. Int. Edit.* **2017**, *56*, 16464-16483; b) P. Tomkins, M. Ranocchiari, J. A. van Bokhoven, *Acc. Chem. Res.* **2017**, *50*, 418-425.

[2] a) V. L. Sushkevich, D. Palagin, M. Ranocchiari, J. A. van Bokhoven, *Science* **2017**, *356*, 523-527; b) S. Grundner, M. A. Markovits, G. Li, M. Tromp, E. A. Pidko, E. J. Hensen, A. Jentys, M. Sanchez-Sanchez, J. A. Lercher, *Nat. Commun.* **2015**, *6*, 7546; c) E. M. Alayon, M. Nachtegaal, M. Ranocchiari, J. A. van Bokhoven, *Chem. Commun.* **2012**, *48*, 404-406; d) K. Narsimhan, K. Iyoki, K. Dinh, Y. Roman-Leshkov, *ACS Cent. Sci.* **2016**, *2*, 424-429; e) A. R. Kulkarni, Z.-J. Zhao, S. Siahrostami, J. K. Nørskov, F. Studt, *Catal. Sci. Tech.* **2018**, *8*, 114-123.; f) D. K. Pappas, A. Martini, M. Dyballa, K. Kvande, S. Teketel, K. A. Lomachenko, R. Baran, P. Glatzel, B. Arstad, G. Berlier, C. Lamberti, S. Bordiga, U. Olsbye, S. Svelle, P. Beato, E. Borfecchia, *J. Am. Chem. Soc.* **2018**, *139*, 15270-15278.

[3] a) D. K. Pappas, E. Borfecchia, M. Dyballa, I. A. Pankin, K. A. Lomachenko, A. Martini, M. Signorile, S. Teketel, B. Arstad, G. Berlier, C. Lamberti, S. Bordiga, U. Olsbye, K. P. Lillerud, S. Svelle, P. Beato, *J. Am. Chem. Soc.* **2017**, *139*, 14961-14975; b) Y. Kim, T. Y. Kim, H. Lee, J. Yi, *Chem. Commun.* **2017**, *53*, 4116-4119.

[4] E. Borfecchia, D. K. Pappas, M. Dyballa, K. A. Lomachenko, C. Negri, M. Signorile, G. Berlier, *Catal. Today* **2018** DOI: 10.1016/j.cattod.2018.07.028 .

[5] a) M. H. Groothaert, P. J. Smeets, B. F. Sels, P. A. Jacobs, R. A. Schoonheydt, *J. Am. Chem. Soc.* **2005**, *127*, 1394-1395; b) H. V. Le, S. Parishan, A. Sagaltchik, C. Göbel, C. Schlesiger, W. Malzer, A. Trunschke, R. Schomäcker, A. Thomas, *ACS Catal.* **2017**, *7*, 1403-1412; c) M. B. Park, S. H. Ahn, A. Mansouri, M. Ranocchiari, J. A. van Bokhoven, *ChemCatChem* **2017**, *9*, 3705-3713; d) V. L. Sushkevich, D. Palagin, J. A. van Bokhoven, *Angew. Chem. Int. Edit.* **2018**, *57*, 8906-8910; e) V. L. Sushkevich, J. A. van Bokhoven, *Catal. Sci. Tech.* **2018**, *8*, 4141-4150; f) B. E. R. Snyder, P. Vanelderen, R. A. Schoonheydt, B. F. Sels, E. I. Solomon, *J. Am. Chem. Soc.* **2018**; *140*, 9236-9243 g) M. A. Newton, A. J. Knorpp, A. B. Pinar, V. L. Sushkevich, D. Palagin, J. A. van Bokhoven, *J. Am. Chem. Soc.* **2018**, *140*, 10090-10093; h) A. J. Knorpp, M. A. Newton, A. B. Pinar, J. A. van Bokhoven, *Ind. Eng. Chem. Res.* **2018**, *57,* 12036-12039

[6] a) M. A. C. Markovits, A. Jentys, M. Tromp, M. Sanchez-Sanchez, J. A. Lercher, *Top. Catal.* **2016**, *59*, 1554-1563; b) G. Li, P. Vassilev, M. Sanchez-Sanchez, J. A. Lercher, E. J. M. Hensen, E. A. Pidko, *J. Catal.* **2016**, *338*, 305-312; c) P. Vanelderen, R. G. Hadt, P. J. Smeets, E. I. Solomon, R. A. Schoonheydt, B. F. Sels, *J. Catal.* **2011**, *284*, 157-164.

[7] a) M. J. Wulfers, S. Teketel, B. Ipek, R. F. Lobo, *Chem. Commun.* **2015**, *51*, 4447-4450; b) B. Ipek, M. J. Wulfers, H. Kim, F. Göltl, I. Hermans, J. P. Smith, K. S. Booksh, C. M. Brown, R. F. Lobo, *ACS Catal.* **2017**, *7*, 4291-4303; c) R. Oord, J. E. Schmidt, B. M. Weckhuysen, *Catal. Sci. Tech.* **2018**, *8*, 1028-1038; d) B. Ipek, R. F. Lobo, *Chem. Commun.* **2016**, *52*, 13401-13404.

[8] a) M. P. Attfield, S. J. Weigel, A. K. Cheetham, *J. Catal.* **1997**, *172*, 274-280; b) A. Kubacka, J. Janas, E. Wloch, B. Sulikowski, *Catal. Today* **2005**, *101*, 139-145.

[9] P. J. Smeets, M. H. Groothaert, R. A. Schoonheydt, *Catal. Today* **2005**, *110*, 303-309.

[10] a) R. Bulanek, B. Wichterlova, Z. Sobalik, J. Tichy, *Appl. Catal. B-Environ.* **2001**, *31*, 13-25; b) P. Nachtigall, M. Davidova, D. Nachtigallova, *J. Phys. Chem. B* **2001**, *105*, 3510-3517; c) R. Bulanek, K. Frolich, P. Cicmanec, D. Nachtigallova, A. Pulido, P. Nachtigall, *J. Phys. Chem. C* **2011**, *115*, 13312-13321.

[11] S. Sklenak, P. C. Andrikopoulos, S. R. Whittleton, H. Jirglova, P. Sazama, L. Benco, T. Bucko, J. Hafner, Z. Sobalik, *J. Phys. Chem. C* **2013**, *117*, 3958-3968.

[12] J. Singh, C. Lamberti, J. A. van Bokhoven, *Chem. Soc. Rev.* **2010**, *39*, 4754-4766.

[13] S. Bordiga, C. Lamberti, F. Bonino, A. Travert, F. Thibault-Starzyk, *Chem. Soc. Rev.* **2015**, *44*, 7262-7341.

[14] a) G. Leofanti, M. Padovan, M. Garilli, D. Carmello, A. Zecchina, G. Spoto, S. Bordiga, G. T. Palomino, C. Lamberti, *J. Catal.* **2000**, *189*, 91-104; b) N. B. Muddada, U. Olsbye, G. Leofanti, D. Gianolio, F. Bonino, S. Bordiga, T. Fuglerud, S. Vidotto, A. Marsella, C. Lamberti, *Dalton Trans.* **2010**, *39*, 8437-8449.

[15] E. Borfecchia, P. Beato, S. Svelle, U. Olsbye, C. Lamberti, S. Bordiga, *Chem. Soc. Rev.* **2018,** *47*, 8097-8133.

[16] S. Grundner, W. Luo, M. Sanchez-Sanchez, J. A. Lercher, *Chem. Commun.* **2016**, *52*, 2553-2556.

[17] S. E. Bozbag, E. M. C. Alayon, J. Pecháček, M. Nachtegaal, M. Ranocchiari, J. A. van Bokhoven, *Catal. Sci. Tech.* **2016**, *6*, 5011-5022.

[18] a) E. Borfecchia, K. A. Lomachenko, F. Giordanino, H. Falsig, P. Beato, A. V. Soldatov, S. Bordiga, C. Lamberti, *Chem. Sci.* **2015**, *6*, 548-563; b) C. Paolucci, A. A. Parekh, I. Khurana, J. R. Di Iorio, H. Li, J. D. A. Caballero, A. J. Shih, T. Anggara, W. N. Delgass, J. T. Miller, F. H. Ribeiro, R. Gounder, W. F. Schneider, *J. Am. Chem. Soc.* **2016**, *138*, 6028-6048; c) C. Paolucci, I. Khurana, A. A. Parekh, S. Li, A. J. Shih, H. Li, J. R. Di Iorio, J. D. Albarracin-Caballero, A. Yezerets, J. T. Miller, W. N. Delgass, F. H. Ribeiro, W. F. Schneider, R. Gounder, *Science* **2017**, *357*, 898; d) A. Martini, E. Borfecchia, K. A. Lomachenko, I. A. Pankin, C. Negri, G. Berlier, P. Beato, H. Falsig, S. Bordiga, C. Lamberti, *Chem. Sci.* **2017**, *8*, 6836-6851; e) K. A. Lomachenko, E. Borfecchia, C. Negri, G. Berlier, C. Lamberti, P. Beato, H. Falsig, S. Bordiga, *J. Am. Chem. Soc.* **2016**, *138*, 12025-12028; f) F. Giordanino, E. Borfecchia, K. A. Lomachenko, A. Lazzarini, G. Agostini, E. Gallo, A. V. Soldatov, P. Beato, S. Bordiga, C. Lamberti, *J. Phys. Chem. Lett.* **2014**, *5*, 1552-1559.

[19] a) V. L. Sushkevich, J. A. van Bokhoven, *Chem. Commun.* **2018**, *54*, 7447-7450; b) G. Turnes Palomino, P. Fisicaro, S. Bordiga, A. Zecchina, E. Giamello, C. Lamberti, *J. Phys. Chem. B* **2000**, *104*, 4064-4073; c) F. X. Llabrés i Xamena, P. Fisicaro, G. Berlier, A. Zecchina, G. T. Palomino, C. Prestipino, S. Bordiga, E. Giamello, C. Lamberti, *J. Phys. Chem. B* **2003**, *107*, 7036-7044.

[20] M. Dyballa, D. K. Pappas, E. Borfecchia, P. Beato, U. Olsbye, K. P. Lillerud, B. Arstad, S. Svelle, *Micropor. Mesopor. Mat.* **2018**, *265*, 112-122.

[21] a) L. S. Kau, D. J. Spira-Solomon, J. E. Penner-Hahn, K. O. Hodgson, E. I. Solomon, *J. Am. Chem. Soc.* **1987**, *109*, 6433-6442; b) E. I. Solomon, D. E. Heppner, E. M. Johnston, J. W. Ginsbach, J. Cirera, M. Qayyum, M. T. Kieber-Emmons, C. H. Kjaergaard, R. G. Hadt, L. Tian, *Chem. Rev.* **2014**, *114*, 3659-3853.

[22] F. Giordanino, P. N. R. Vennestrøm, L. F. Lundegaard, F. N. Stappen, S. Mossin, P. Beato, S. Bordiga, C. Lamberti, *Dalton Trans.* **2013**, *42*, 12741-12761.

[23] G. T. Palomino, S. Bordiga, C. Lamberti, A. Zecchina, C. O. Arean, *Stud. Surf. Sci. Catal.* **2002**, *142*, 199-206.

[24] S. Brunauer, P. H. Emmett, E. Teller, *J. Am. Chem. Soc.* **1938**, *60*, 309-319.

[25] S. Bordiga, E. Groppo, G. Agostini, J. A. van Bokhoven, C. Lamberti, *Chem. Rev.* **2013**, *113*, 1736-1850.

[26] D. Bellet, B. Gorges, A. Dallery, P. Bernard, E. Pereiro, J. Baruchel, *J. Appl. Crystallogr.* **2003**, *36*, 366-367.

[27] V. A. Sole, E. Papillon, M. Cotte, P. Walter, J. Susini, *Spectrochim. Acta B* **2007**, *62*, 63-68.

[28] B. Ravel, M. Newville, *J. Synchrotron Radiat.* **2005**, *12*, 537-541.

10.1002/cctc.201801542

WILEY-VCH

Entry for the Table of Contents (Please choose one layout)

Layout 1:

FULL PAPER

Reducibility is the key: Cu-FER zeolites show a high methanol yield depending on the Cu loading and reaction conditions. *In situ* HERFD XANES and IR of adsorbed CO evidence how the sample reducibility depends on the loading as well as location of Cu in the framework, ultimately affecting the activity in the reaction.

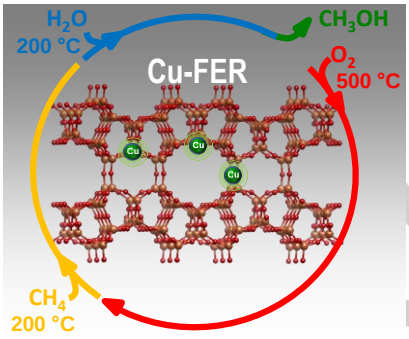

*Author(s), Corresponding Author(s)**

Page No. – Page No.

Title